PERGAMON

International Journal of Solids and Structures 37 (2000) 6343–6360

INTERNATIONAL JOURNAL OF SOLIDS and STRUCTURES

www.elsevier.com/locate/ijsolstr

Characteristic state plasticity for granular materials Part I: Basic theory

Steen Krenk

Department of Structural Engineering and Materials, Technical University of Denmark, DK-2800, Lyngby, Denmark

Received 12 May 1999; in revised form 20 September 1999

Abstract

A non-associated plasticity theory is developed for granular materials based on the concept of a characteristic stress state of vanishing incremental dilation. The theory makes use of a common format for yield surface and flow potential, representing the surfaces in terms of stress invariants and a single shape function for each. The flow potential surface is determined by an approximate friction hypothesis. Plastic work hardening is introduced in a linear invariant form, that permits dilation before the ultimate state, by including the work associated with shape change in addition to the traditional contribution from volume change. The model is fully three-dimensional and is defined by only six parameters: two for elastic stiffness, one for plastic stiffness, two for the shape of yield and plastic potential surfaces, and one for the dilation at failure. Typical material response is illustrated, while model calibration and its ability to represent experimental data are discussed in Part II.

Keywords: Plasticity; Granular materials; Soil mechanics

1. Introduction

In granular materials with hard particles the main deformation mechanism is sliding between the grains under the effect of friction. The ratio of shear to normal stress therefore plays a dominant role in the mechanical behavior. In the formulation of a plasticity theory for granular materials, this suggests self-similar families of yield surfaces and plastic potential surfaces, where only the stress ratios appear. It is a common experience that friction effects lead to non-associated behavior, and a plasticity theory therefore requires identification of yield surface, plastic potential and a suitable hardening mechanism.

Traditionally, plasticity theories are formulated in stress space, and it is therefore important to

E-mail address: sk@bkm.dtu.dk (S. Krenk).

0020-7683/00/$ - see front matter
PII: S0020-7683(99)00278-4

identify characteristics of the deformation behavior that can be described in stress space, without explicit reference to the state of deformation. Fig. 1 shows results of a standard triaxial test on two sand samples with the same type of grains, but with different void ratio e. The axial strain is denoted by ε_1 and the volumetric strain by ε_v. The confining stress is σ_3, and the difference between maximum and minimum principal stress is $q = \sigma_1 - \sigma_3$. The volumetric strain shows a typical transition from initial contraction to dilation, reaching an approximate constant rate of dilation before reaching the maximum stress difference level.

The point of transition from contraction to dilation will be termed the *characteristic state*, while the state corresponding to maximum excess stress will be termed the *ultimate state*. The characteristic and ultimate states are indicated for both loose and dense material on each graph. It is seen that the characteristic state corresponds closely to identical values of q for both materials, while the ultimate capacity q_u is higher for the dense material. This observation, also supported by numerous other test results, suggests that a plasticity theory for granular materials should include explicit recognition of the characteristic state in stress space, while the ultimate state depends on the state of deformation. This was recognized in the early work of Roscoe and Schofield (1963) and Roscoe and Burland (1968) in the development of critical state theory for soils. Classical critical state theory was developed in terms of a two-dimensional stress space with mean stress p and maximum shear stress $\frac{1}{2}q$. The ultimate stress states are located on the critical line $q/p = M$ corresponding to a state of plastic shear without dilation (Schofield and Wroth, 1968). While representing some of the basic features of granular materials well, the critical state theory has a number of shortcomings, such as the two-dimensional basis of the theory, the assumption of an associated flow rule, and lack of dilatation before failure.

In the present theory, the concepts from classical critical state theory are generalized to provide a non-associated hardening plasticity theory in terms of stress invariants. The theory is formulated in terms of a family of smooth self-similar yield surfaces that satisfy the no-tension condition and an independent plastic flow potential derived approximately from a friction hypothesis, thus generalizing a preliminary associated theory (Krenk, 1997). The shape yield surface and the plastic flow potential are each determined by a single parameter, specifying the aspect ratio of the surface in principal stress space. The aspect ratio of the plastic potential surface can alternatively be expressed as the inclination of the line in a p, q-diagram marking the transition from contraction to dilation. While the classical critical state theory identifies this state with the ultimate state, the ultimate state is defined independently in the

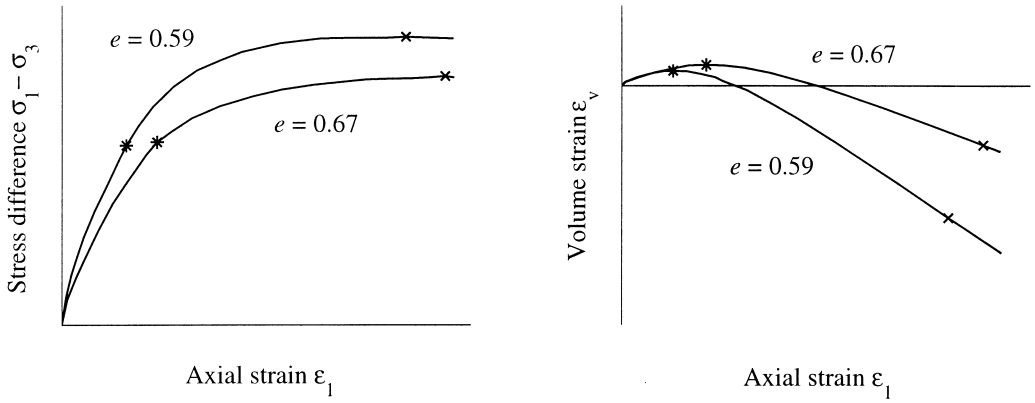

Fig. 1. Tests on loose and dense Eastern Scheldt sand with confining stress $\sigma_3 = 640$ Pa, (adapted from Andersen et al., 1997). (a) Stress difference q, (b) volumetric strain ε_v.

present theory and typically corresponds to dilation. The development of plastic strain is controlled by a linear work-hardening rule, in which, contributions from dilation and shear deformation are included with separate weights. The relative weight on the shear deformation in the hardening rule determines the plastic strain ratio and the shear to mean stress ratio of the ultimate stress states. Thus, the plasticity effects of the present theory are specified by only four parameters: a plastic stiffness, the inclination M_c of the characteristic line, the inclination M_u of the ultimate line, and the inclination M_f of the line to the point of maximum width of the yield surface. All parameters of the model can be determined from the stress–strain results of a standard triaxial test by a non-linear procedure described by Ahadi and Krenk (1999) in a sequel to the present paper.

2. The general surface format

Fig. 2(a) shows a typical isotropic yield surface in principal stress space σ_1, σ_2, σ_3. The stresses are positive in compression, and when the material is assumed to be without cohesion, the yield surface is entirely within the first octant. The yield surface is assumed to be isotropic, and when the yield mechanism is friction, the yield surface will only depend on the ratio between the stress components. With these assumptions only a single yield surface is needed, as it will grow in a self-similar way. Similarly, a surface with isotropic symmetry is needed for the plastic flow potential. In the present theory, the same general format is used for both surface families, although they have distinctly different shape.

The surface is generated by a family of curves in the octahedral planes, of which one is shown in Fig. 2(b). There is experimental evidence that the failure envelope is of rounded triangular shape, e.g. Lade and Duncan (1975). The minimum requirement of the octahedral curves therefore, is a triangular format permitting the specification of the "corner" and the midpoint of the "side" of the triangle. Several such formats are available, e.g. Lade and Duncan (1975), Lade (1977), Matsuoka and Nakai (1985), Haythornwaithe (1984, 1985, 1992), Weidner (1990), Krenk (1996, 1997). All these formats have

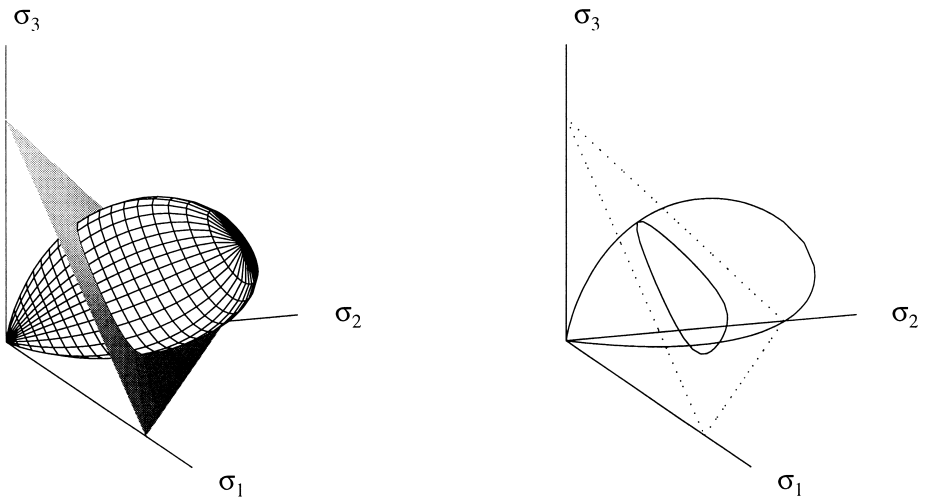

Fig. 2. (a) Yield surface in principal stress space, (b) generating curves in octahedral and meridian planes.

the common feature that the triangularity is generated via the third invariant of the total or deviatoric stresses. The next section describes the structure of the simple cubic format with two parameters, and then, introduce a suitable format of the meridian curves to define the yield surface and plastic flow potential.

2.1. The octahedral contours

In the formulation of the model, it is convenient to use the mean stress p and the deviatoric stresses s_{ij},

$$p = \frac{1}{3}\sigma_{ii}, \qquad s_{ij} = \sigma_{ij} - p\delta_{ij} \tag{1}$$

The simplest form of an octahedral contour that satisfies symmetry with respect to the three principal deviator stress components (s_1, s_2, s_3) is the cubic polynomial

$$(s_1 + d)(s_2 + d)(s_3 + d) = \eta d^3 \tag{2}$$

where the stress parameter d determines the size of the circumscribing triangle, and η is a non-dimensional shape parameter (Krenk, 1996). The family of curves corresponding to parameter values $0 \le \eta \le 1$ are illustrated in Fig. 3. For $\eta = 0$, the curve is composed of the three lines $s_j = -d$, $j = 1, 2, 3$. The relevant part is the isosceles triangle corresponding to the corner points $(s_1, s_2, s_3) = (2d, -d, -d)$ etc. and midside points $(s_1, s_2, s_3) = (-d, \frac{1}{2}d, \frac{1}{2}d)$ etc. The center $s_1 = s_2 = s_3 = 0$ corresponds to $\eta = 1$, and for any $0 < \eta < 1$, equation (2) defines a convex contour inside the triangle. For small values of η, the contour is nearly triangular, and for η close to 1, the curve approaches circular shape. Eq. (2) also generates three open branches, located symmetrically inside the exterior corner regions of the lines $s_j = -d$, $j = 1, 2, 3$. These branches are not part of the constitutive model, but it is important to know their existence when developing numerical integration algorithms, in which, the stress point may temporarily be located outside the yield surface.

The cubic Eq. (2) is conveniently written in terms of the deviatoric stress invariants

$$J_2 = \frac{1}{2}s_{ij}s_{ij} = \frac{1}{2}\left(s_1^2 + s_2^2 + s_3^2\right) = -(s_2s_3 + s_3s_1 + s_1s_2) \tag{3}$$

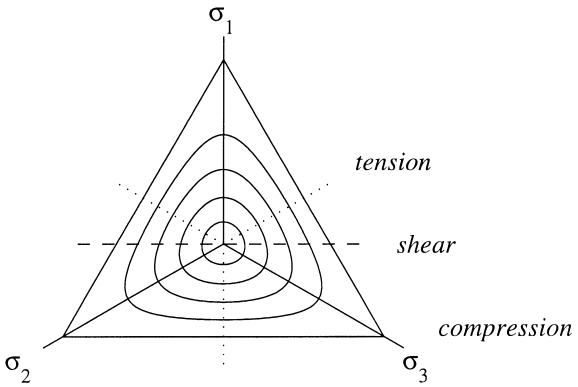

Fig. 3. Smooth triangular contours with identification of triaxial "compression", "tension" and "shear".

and

$$J_3 = \frac{1}{3} s_{ij} s_{jk} s_{ki} = s_1 s_2 s_3 \tag{4}$$

When using the fact that the sum of the deviator stresses is zero, Eq. (2) takes the form

$$J_3 - dJ_2 + (1-\eta)d^3 = 0 \tag{5}$$

Thus, in any octahedral plane, the contour is given in terms of a size parameter d, defining the circumscribing triangle, and a shape parameter η, determining the *relative size*, and thereby the shape of the contour.

In the state of triaxial shear $\sigma_2 = \frac{1}{2}(\sigma_1 + \sigma_3)$, and thus, $s_3 = -s_1$ and $s_2 = 0$. In this stress state $J_3 = 0$, and the Eq. (5) takes the particularly simple form

$$J_2 = (1-\eta)d^2, \quad \text{triaxial shear} \tag{6}$$

When it is observed that $J_2^{1/2}$ is a measure of the distance from the isostatic axis, it is seen, that the parameter

$$\gamma = (1-\eta)^{1/2}, \quad 0 \le \gamma \le 1 \tag{7}$$

is a direct measure of the relative width of the contour, $\gamma = J_2^{1/2}/d$.

2.2. Parameter representation of the surface

A parametric representation of the yield surface $f(\sigma_j) = 0$ is obtained by introducing the Lode angle

$$\cos 3\theta = -3\frac{\sqrt{3}}{2}\frac{J_3}{J_2^{3/2}} \tag{8}$$

Eq. (5) can then be expressed as a cubic in the radius in the octahedral plane, $s = (s_{ij}s_{ij})^{1/2} = (2J_2)^{1/2}$. The solution of this cubic equation is, see e.g. Krenk (1996),

$$s = \frac{\sqrt{\frac{3}{2}}\gamma d}{\cos\left(\frac{1}{3}\arccos(\gamma \cos 3\theta)\right)} \tag{9}$$

Finally, the principal stresses can be expressed in terms of mean stress p, the radius in the deviatoric plane s, and the Lode angle θ,

$$\begin{bmatrix} \sigma_1 \\ \sigma_2 \\ \sigma_3 \end{bmatrix} = p \begin{bmatrix} 1 \\ 1 \\ 1 \end{bmatrix} + s\sqrt{\frac{2}{3}} \begin{bmatrix} -\cos\theta \\ \cos\left(\theta - \frac{1}{3}\pi\right) \\ \cos\left(\theta + \frac{1}{3}\pi\right) \end{bmatrix} \tag{10}$$

This representation was used to plot the surfaces.

3. Yield function and plastic flow potential

The shape of the yield surface and the plastic flow potential surface are determined by prescribing the size $d = d(p)$ of the circumscribing triangle, and the relative size $\gamma = \gamma(p)$ as functions of mean stress p. In addition to analytical convenience, this approach has the advantage that the product $\gamma(p)d(p)$ directly defines the contour of the surface in the three triaxial shear planes. An alternative formulation in which the compression and tension meridians are defined explicitly in terms of p is less convenient, see e.g. Krenk (1996).

In the present theory, the size of the circumscribing triangle is assumed to be proportional to the mean stress p,

$$d(p) = \alpha p \tag{11}$$

corresponding to an ideal friction material where only the ratio between the stresses are important. If this assumption is introduced into the surface format (5), interpolation of the compression and tension meridians of the Coulomb friction criterion leads to the Matsuoka and Nakai (1985) criterion. This corresponds to a circumscribing triangle that is slightly inside the coordinate planes of the principal stress space, i.e. $\alpha < 1$ (Krenk, 1996). However, the work of Lade and Duncan (1975), Lade (1977) and Lade and Kim (1995) has demonstrated, that material behavior corresponds well to a surface format in which, the circumscribing triangle is the intersection of the octahedral plane with the coordinate planes in principal stress space. This assumption, corresponding to $\alpha = 1$ and thereby

$$d(p) = p \tag{12}$$

will be adopted in the following. However, the parameter α can be retained in the format and used to control the opening of the surface with minimal extra effort.

In the case of $\alpha = 1$, the yield function can be written in terms of the third total stress invariant

$$I_3 = \det(\sigma_{ij}) = \sigma_1\sigma_2\sigma_3 = J_3 - pJ_2 + p^3 \tag{13}$$

This leads to the yield function

$$f(\boldsymbol{\sigma}) = -J_3 + pJ_2 - p^3\big(1 - \eta_f(p)\big) = -I_3 + p^3\eta_f(p) \tag{14}$$

determined completely by the shape function $\eta_f(p)$. The plastic deviator strains are assumed to be associated, while the volumetric strain component is non-associated. This assumption corresponds to adopting identical shape deviator contours for the plastic potential and yield surface through the same stress state, and thus, the plastic potential is of the form

$$g(\boldsymbol{\sigma}) = -J_3 + pJ_2 - p^3\big(1 - \eta_g(p)\big) = -I_3 + p^3\eta_g(p) \tag{15}$$

where the shape is determined by the function $\eta_g(p)$.

3.1. The yield surface

There does not appear to be a theory for the shape of the yield function of granular materials. Experiments suggest a rounded drop-like shape. In the present theory it is assumed that, the yield surface approaches the circumscribing triangle for small p and is closed for a value of $p = p_f$, defining the current size of the yield function. This implies that the function $\eta(p/p_f)$ should increase monotonically from 0 to 1, when the argument p/p_f increases from 0 to 1. A smooth transition is

accomplished by the power function

$$\eta_f(p) = \left(p/p_f\right)^m \tag{16}$$

by which, the shape of the fully three-dimensional yield function has been reduced to a single non-dimensional parameter m.

The yield surface is illustrated in Fig. 2, and the traces in the triaxial shear plane and a plane containing the vertical principal axis and bisecting the angle between the two horizontal axes in the principal stress space, are shown in Fig. 4 for different values of the exponent m. For increasing exponent m, the "diameter" of the yield surface increases, and it becomes increasingly flat at the end $p \simeq p_f$. The shape parameter m is assumed to be constant for any given material, while the parameter p_f controls the current size of the yield surface and is determined by a hardening relation.

3.2. The plastic potential

In contrast to the yield surface, several mechanically based theories have been proposed for the shape of the plastic flow potential surfaces, e.g. the Taylor hypothesis used in the original Cam–Clay theory (Schofield and Wroth, 1968), the constant energy ratio theory proposed by Rowe (1962) and de Jong (1976), and a generalized Coulomb friction theory with state dependent angle of dilation (Krenk, 1998). In the following, an approximate theory is developed that improves on the classic Taylor hypothesis, while leading to a very simple shape function $\gamma_g(p)$.

The derivation refers to stress states of triaxial shear and makes use of the p, q stress format with $q = \sigma_1 - \sigma_3$. In the state of triaxial shear, the middle principal stress is the mean of the two others, and thus in this state of stress, $p = \frac{1}{2}(\sigma_1 + \sigma_3)$. The conjugate plastic strain increments are $\mathrm{d}\varepsilon_v^p$, $\mathrm{d}\varepsilon_q^p$. Assuming that the deformation takes place in the plane defined by the maximum and minimum stress components, the plastic work is

$$p\mathrm{d}\varepsilon_v^p + q\mathrm{d}\varepsilon_q^p = \mathrm{d}W^p \tag{17}$$

and after division by $p\mathrm{d}\varepsilon_q$,

$$\frac{q}{p} + \frac{\mathrm{d}\varepsilon_v^p}{\mathrm{d}\varepsilon_q^p} = \frac{\mathrm{d}W^p}{p\mathrm{d}\varepsilon_q^p} \tag{18}$$

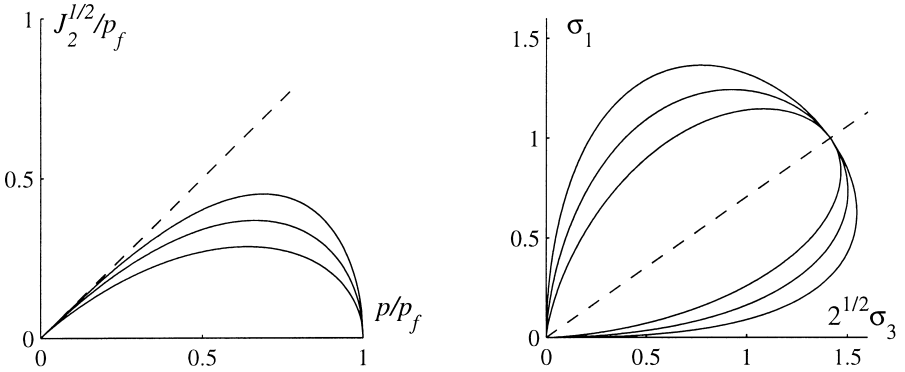

Fig. 4. Yield surface for $m = 0.5, 0.9, 1.5$. (a) Shear plane contour, (b) meridian curves.

The plastic strain increment vector $(d\varepsilon_v^p, d\varepsilon_q^p)$ is orthogonal to the plastic potential surface, and thus,

$$\frac{d\varepsilon_v^p}{d\varepsilon_q^p} = -\frac{dq}{dp} \tag{19}$$

This relation is used to eliminate the plastic strain increment ratio from Eq. (18), giving

$$\frac{q}{p} - \frac{dq}{dp} = \frac{dW^p}{p d\varepsilon_q^p} \tag{20}$$

Various hypotheses regarding the right side of this equation leads to different plastic flow potential contours.

In the classic Taylor hypothesis it was concluded from an approximate analysis of a shear box that the plastic work is of the form $dW^p = Mp d\varepsilon_q^p$, where M is a parameter, representative of the material friction. This result rests on the assumption that the mean stress p can be assumed to be representative for the normal stress on an active shear plane. Clearly, this assumption breaks down, when one of the principal stresses becomes negative. It will therefore be replaced by the more consistent assumption

$$dW^p = 2n\sigma_{min} d\varepsilon_q^p \tag{21}$$

where the minimum principal stress has been used as the representative stress on active shear planes. In the present state of triaxial shear $\sigma_{min} = p - \frac{1}{2}q$, and the energy Eq. (20) then takes the form

$$\frac{q}{p} - \frac{dq}{dp} = n\left(2 - \frac{q}{p}\right) \tag{22}$$

Now, in triaxial shear $q/p = 2J_2^{1/2}/p = 2\gamma_g(p)$, and the differential equation (22) can be integrated to give

$$\gamma_g(p) = 1 - (p/p_g)^n \tag{23}$$

Like in the case of the yield function this is a simple power function, but this time for $1 - \gamma_g$ and not for η_f.

The traces of the plastic potential in the triaxial shear plane and a plane containing the vertical

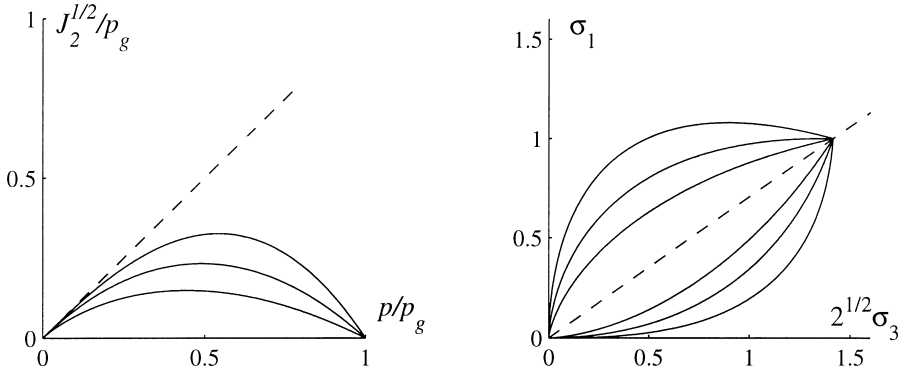

Fig. 5. Plastic potential surface for $n = 0.5, 0.9, 1.5$. (a) Shear plane contour, (b) meridian curves.

principal axis and bisecting the angle between the two horizontal axes in the principal stress space are shown in Fig. 5 for different values of the exponent n. In spite of the approximation involved in using σ_{min} as the representative normal stress on active shear planes, the curves look remarkably similar to those resulting from the more detailed analysis involving a state dependent angle of dilation presented in Krenk (1998). A three-dimensional illustration of the plastic flow potential in principal stress space is given in Fig. 6(a), with the generators of the surface shown in Fig. 6(b).

3.3. Shape parameters and characteristic state

Most of the experimental data are available from triaxial tests in which only the axial stress σ_1 and the cell pressure $\sigma_2 = \sigma_3$ are varied. It is therefore convenient to express the parameters n and m in a form where they can be determined from triaxial tests, using the stress variables p and $q = \sigma_1 - \sigma_3$. In terms of these variables, the deviator stress invariants are $J_2 = \frac{1}{3}q^2$ and $J_3 = \frac{2}{27}q^3$, where q is positive for triaxial compression and negative for triaxial tension. For these two special stress conditions the plastic potential (15) is expressed as

$$g(p, q) = -\frac{2}{27}q^3 + \frac{1}{3}q^2 p - \big(1 - \eta_g\big)p^3 \tag{24}$$

with $\eta_g = 1 - \gamma_g^2$. Apart from the function $\eta_g(p)$, the potential function is homogeneous of degree three in the stresses. This gives the differential relation

$$p\frac{\partial g}{\partial p} + q\frac{\partial g}{\partial q} = 3g + p^4\frac{\mathrm{d}\eta_g}{\mathrm{d}p} \tag{25}$$

This relation leads to a simple explicit formula for the parameter n in terms of the slope of the characteristic state line $M_c = (q/p)_c$.

The characteristic state is described by the zero incremental dilation condition $\mathrm{d}\varepsilon_v = 0$. In the following, this condition is used for the plastic volumetric strain increment $\mathrm{d}\varepsilon_v^p$. Thus, $\partial g/\partial p = 0$ at the characteristic line. At any particular state of yielding, the parameters p_f and p_g take values such that

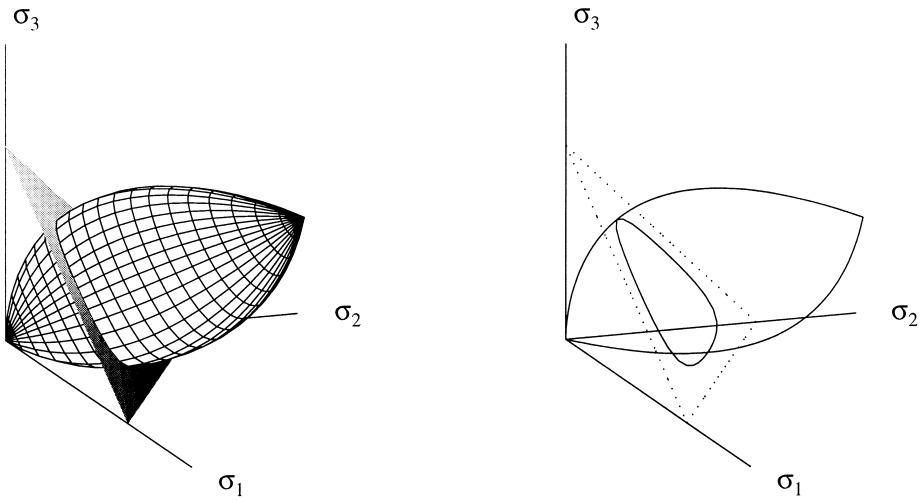

Fig. 6. Plastic potential surface in principal stress space, (b) generating curves in octahedral and meridian planes.

$f(\sigma) = g(\sigma) = 0$. This implies that $\eta_g = \eta_f = \eta$, and for a given state of stress, η can be evaluated directly from the yield function, without evaluating p_g or p_f.

At the characteristic state, the differential relation (25) takes the simpler form

$$\frac{q}{p^3}\frac{\partial g}{\partial q} = p\frac{\mathrm{d}\eta_g}{\mathrm{d}p} \tag{26}$$

The right-hand side is evaluated by differentiation of the function $\eta_g(p)$ for the plastic potential, given by Eq. (23).

$$p\frac{\mathrm{d}\eta_g}{\mathrm{d}p} = -2\gamma_g p\frac{\mathrm{d}\gamma_g}{\mathrm{d}p} = 2n\gamma_g(1-\gamma_g) \tag{27}$$

The left hand side of Eq. (26) is determined by differentiation of the flow potential in the form (24),

$$\frac{q}{p^3}\frac{\partial g}{\partial q} = \frac{2}{9}M_c^2(3 - M_c) \tag{28}$$

where $M_c = (q/p)_c$ is the inclination of the characteristic line in a p, q-plot of triaxial compression. The parameter n is then determined as

$$n = \frac{1}{9}\frac{M_c^2(3 - M_c)}{\gamma_c(1-\gamma_c)} \tag{29}$$

where γ_c is the value of γ at the characteristic state line, determined from the relation $g(p, q) = 0$ as

$$\gamma_c^2 = \frac{1}{3}M_c^2\left(1 - \frac{2}{9}M_c\right) \tag{30}$$

These two relations determine the parameter n explicitly from the inclination M_c of the characteristic line in triaxial compression. Naturally, the parameter n can also be determined by different expressions from the critical state of stress on other meridians, e.g. triaxial shear or triaxial tension.

A similar derivation leads to an expression of the yield function parameter m in terms of the inclination $M_f = (q/p)_f$ of a line from origo to the maximum point of the yield contour in a p,q-plot of a triaxial compression test. Under triaxial test conditions, the yield function (14) is

$$f(p, q) = -\frac{2}{27}q^3 + \frac{1}{3}q^2 p - (1 - \eta_f)p^3 \tag{31}$$

with $\eta_f(p) = (p/p_f)^m$. Apart from the function $\eta_f(p)$, the yield function is homogeneous of degree three in the stresses. This gives the differential relation

$$p\frac{\partial f}{\partial p} + q\frac{\partial f}{\partial q} = 3f + \frac{\mathrm{d}\eta_f}{\mathrm{d}p}p^4 = m\eta_f p^3 \tag{32}$$

where the yield condition $f = 0$ has been used.

At the maximum point of the yield contour in a p,q-plot, $\partial f/\partial p = 0$. Eq. (32) then implies, that the parameter m can be expressed as

$$m = \frac{q\partial f/\partial q}{\eta_f p^3} \tag{33}$$

When η_f is eliminated by use of the condition $f(p, q) = 0$, this expression reduces to

$$m = \frac{6M_f^2}{(3 - M_f)(3 + 2M_f)} \tag{34}$$

where $M_f = (q/p)_f$ is the inclination of the line to the maximum point of the yield contour in a p, q-plot.

The geometric interpretation of the parameters M_c and M_f is illustrated in Fig. 7, using the values $M_c = 1.2$ and $M_f = 0.9$, representative of dense sand. The characteristic line $q = M_c p$ shown in Fig. 7(a) separates contracting and dilating states of stress and can be determined directly from a triaxial test. The parameter M_f, defining the shape of the yield surface, does not seem to have a similar direct physical interpretation. Experimental results by Andersen et al. (1997) indicate that $M_f < M_c$, and it is demonstrated by Ahadi and Krenk (1999) that an empirical relation can be developed for the parameter M_f in terms of the slope M_c of the characteristic line and the rate of dilation prior to failure.

4. Stress–strain relations

In non-associated plasticity theory, the plastic strain increment is proportional to the gradient of the plastic potential,

$$\mathrm{d}\boldsymbol{\varepsilon}^p = \mathrm{d}\chi \frac{\partial g}{\partial \boldsymbol{\sigma}} \tag{35}$$

When the incremental elastic stiffness tensor is denoted by $\mathbf{C}$, the total strain increment is

$$\mathrm{d}\boldsymbol{\varepsilon} = \mathbf{C}^{-1}\mathrm{d}\boldsymbol{\sigma} + \frac{\partial g}{\partial \boldsymbol{\sigma}}\,\mathrm{d}\chi \tag{36}$$

The factor $\mathrm{d}\chi$ is determined by plastic hardening via the consistency condition,

$$\mathrm{d}f = \frac{\partial f}{\partial \boldsymbol{\sigma}}\mathrm{d}\boldsymbol{\sigma} - H\,\mathrm{d}\chi = 0 \tag{37}$$

where the hardening parameter H is defined as

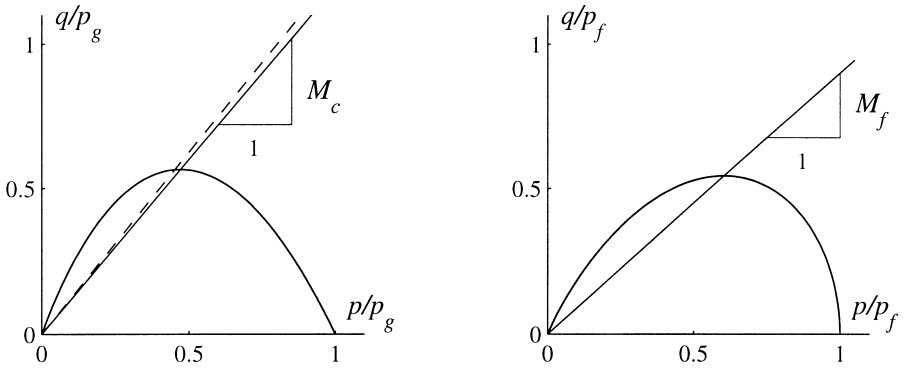

Fig. 7. p,q-representation of (a) flow potential with $M_c = (q/p)_c$, (b) yield surface with $M_f = (q/p)_f$.

$$H = -\frac{\partial f}{\partial p_f}\frac{\mathrm{d}p_f}{\mathrm{d}\chi} = H_1 H_2 \tag{38}$$

The factor $H_1 = -\partial f/\partial p_f$ gives the dependence of the yield surface on the size parameter p_f, while $H_2 = \partial p_f/\partial\chi$ describes the plastic hardening via the hardening rule developed below.

The relation between the stress increment $\mathrm{d}\boldsymbol{\sigma}$ and the total strain increment $\mathrm{d}\boldsymbol{\varepsilon}$ is determined from Eqs. (36) and (37). The factor $\mathrm{d}\chi$ follows from multiplication of Eq. (36) with $\partial f/\partial\boldsymbol{\sigma}\mathbf{C}$ and subtraction of Eq. (37). The elasto-plastic stiffness tensor is then determined from Eq. (36) as

$$\mathbf{C}_{ep} = \mathbf{C} - \frac{(\mathbf{C}\partial g/\partial\boldsymbol{\sigma})(\partial f/\partial\boldsymbol{\sigma}\mathbf{C})}{H + \partial f/\partial\boldsymbol{\sigma}\mathbf{C}\partial g/\partial\boldsymbol{\sigma}} \tag{39}$$

In the following the material properties are described in tensor format, separating volumetric and deviatoric parts, while the elasto-plastic stiffness is derived from Eq. (39) in six-component vector format.

4.1. Stiffness parameters and hardening rule

The material stiffness and hardening parameters are formulated in terms of volume and deviator strains,

$$\varepsilon_v = \varepsilon_{ii}, \qquad e_{ij} = \varepsilon_{ij} - \frac{1}{3}\varepsilon_v\delta_{ij} \tag{40}$$

The elastic part of the deviator strains is assumed to be proportional to the deviator stresses, $s_{ij} = 2Ge^e_{ij}$, with constant shear modulus G.

A linear relation between the specific volume and the logarithm of the mean stress is assumed in the elastic and the elasto-plastic states, i.e.

$$\mathrm{d}\varepsilon^e_v = \frac{\kappa}{p}\mathrm{d}p, \qquad \mathrm{d}\varepsilon_v = \frac{\lambda}{p}\mathrm{d}p \tag{41}$$

where the two non-dimensional flexibility parameters κ and λ are the inclination of the $\varepsilon_v - \ln p$ line of isotropic compression in the elastic and the elasto-plastic state, respectively.

The plastic volume strain increment $\mathrm{d}\varepsilon^p_v = \mathrm{d}\varepsilon_v - \mathrm{d}\varepsilon^e_v$ in isotropic elastic–plastic compression is then related to the mean stress increment by

$$\mathrm{d}p = \frac{p}{\lambda - \kappa}\mathrm{d}\varepsilon^p_v \tag{42}$$

In the case of elasto-plastic isotropic loading, p may be replaced by p_f, and thus, relation (42) defines the hardening in this specific case.

In the classical critical state theory, hardening is derived from volume changes alone (Schofield and Wroth, 1968). Thus, hardening stops, and unlimited plastic deformation can take place, once the critical state of zero incremental dilation is reached. In the present model, the work of the deviatoric stresses is assumed to give an additive contribution to the hardening. Thus, for a general stress path relation (42) is generalized to give the increment of p_f in terms of a weighted sum of the volumetric and deviatoric parts of the plastic work,

$$\mathrm{d}p_f = \frac{1}{\lambda - \kappa}\left(p\mathrm{d}\varepsilon^p_v + ws_{ij}\mathrm{d}e^p_{ij}\right) \tag{43}$$

where w is a non-dimensional weight parameter. At the ultimate state $\mathrm{d}p_f = 0$, and deformation proceeds without further hardening. In this state, the plastic work of the deviatoric stresses $s_{ij}\,\mathrm{d}e_{ij}^p$ is positive, and for $w > 0$, the ultimate state therefore corresponds to a negative value of $\mathrm{d}\varepsilon_v^p$, i.e. to dilation. The ultimate state and the weight parameter w are discussed further in Section 4.3.

The factor H_1 from Eq. (38) follows directly from the yield function (14) by differentiation,

$$H_1 = -\frac{\partial f}{\partial p_f} = mp^2\eta^{(m+1)/m} \tag{44}$$

The hardening factor H_2 is found by inserting the plastic strain increment (35) into the hardening rule (43), and substituting the plastic potential function (15).

$$H_2 = \frac{\mathrm{d}p_f}{\mathrm{d}\chi} = \frac{1}{\lambda-\kappa}\left(p\frac{\partial p}{\partial p} + ws_{ij}\frac{\partial g}{\partial s_{ij}}\right) = \frac{p}{\lambda-\kappa}\left[(1-w)\left(J_2 - 3\gamma^2p^2\right) + 2n\gamma(1-\gamma)p^2\right] \tag{45}$$

The hardening parameter H has now been determined as a function of the stress invariants p and J_2.

4.2. Weight parameter and ultimate state

In the ultimate state plastic deformation can proceed without further plastic hardening, and thus, the ultimate state is determined by the condition of vanishing increment of the weighted plastic work in Eq. (43). In turn this corresponds to $H_2 = 0$, and by reduction of the expression (45) the weight factor w is determined as

$$w = 1 - n\frac{9\gamma_u(1-\gamma_u)}{M_u^2(3-M_u)} \tag{46}$$

where $M_u = (q/p)_u$ is the stress ratio in the ultimate state, and γ_u refers to γ evaluated at the stress state $(p, q)_u$. The fraction in Eq. (46) is seen to be similar to the inverse of the expression (29), used to calculate the exponent $n = n(M_c)$ corresponding to the critical inclination M_c. The only difference is that, in Eq. (46) the inclination is M_u, corresponding to the ultimate line. Thus, the formula for the weight factor w can be written in the form

$$w = 1 - \frac{n(M_c)}{n(M_u)} \tag{47}$$

This formula is very convenient for numerical implementation, as it simply requires evaluation of the expression (29) for the two inclinations M_c and M_u. In practice, the difference between the inclinations M_c and M_u of the characteristic and ultimate line is small, as illustrated in Fig. 7(a) by the dotted ultimate line $q = M_u p$ with $M_u = 1.25$.

It follows from the formula (47) that the weight w is determined explicitly from the two directly measurable parameters $M_c = (q/p)_c$ and $M_u = (q/p)_u$. However, the small difference between M_c and M_u for many granular materials makes determination of the weight w from Eq. (47) very inaccurate. It is therefore important to realize that the intersection of the ultimate line $q = M_u p$ with the plastic potential determines the direction of the normal and thereby the ratio between the plastic strain increments $\mathrm{d}\varepsilon_v^p$ and $\mathrm{d}\varepsilon_q^p = \frac{2}{3}(\mathrm{d}\varepsilon_1^p - \mathrm{d}\varepsilon_3^p)$ at the ultimate state. The mathematical relation follows from Eq. (43) by observing that the deviatoric plastic work in a triaxial compression test is $s_{ij}\,\mathrm{d}e_{ij}^p = q\mathrm{d}\varepsilon_q^p$. Thus, the ultimate state condition $\mathrm{d}p_f = 0$ gives the relation

$$wM_u = -\left(\frac{\mathrm{d}\varepsilon_v^p}{\mathrm{d}\varepsilon_q^p}\right)_u \tag{48}$$

It is seen that the weight parameter w controls the strain rate ratio $\mathrm{d}\varepsilon_v^p/\mathrm{d}\varepsilon_q^p$, and thereby the volumetric rate of strain, at the ultimate state. In the ultimate state, the elastic strains are usually negligible compared to the plastic strains, and thus, the plastic strain rate ratio on the right-hand side of Eq. (48) is approximately equal to the total strain rate ratio. In the calibration of the model, described by Ahadi and Krenk (1999), the asymptotic ultimate strain rate relation (48) is used iteratively to determine the parameter w.

4.3. Stiffness matrices

For numerical computations it is convenient to express the incremental stress–strain relations in the six-component format with the stress vector

$$\boldsymbol{\tau} = (\sigma_x, \sigma_y, \sigma_z, \tau_{yz}, \tau_{zx}, \tau_{xy}) \tag{49}$$

and the strain vector

$$\boldsymbol{\gamma} = (\varepsilon_x, \varepsilon_y, \varepsilon_z, \gamma_{yz}, \gamma_{zx}, \gamma_{xy}) \tag{50}$$

with angular shear strains $\gamma_{yz} \ldots$. The corresponding elastic tangent stiffness matrix is

$$\mathbf{C} = G\begin{bmatrix} a & b & b & & & \\ b & a & b & & & \\ b & b & a & & & \\ & & & 1 & & \\ & & & & 1 & \\ & & & & & 1 \end{bmatrix} \tag{51}$$

with the non-dimensional parameters

$$a = \frac{p}{\kappa G} + \frac{4}{3}, \qquad b = \frac{p}{\kappa G} - \frac{2}{3} \tag{52}$$

In the six-component format, the stress invariant I_3 used in the yield function (14) and the plastic potential (15) is

$$I_3 = \sigma_x\sigma_y\sigma_z + 2\tau_{yz}\tau_{zx}\tau_{xy} - \left(\sigma_x\tau_{yz}^2 + \sigma_y\tau_{zx}^2 + \sigma_z\tau_{xy}^2\right) \tag{53}$$

The gradient of the yield function (14) takes the form

$$\frac{\partial f(\boldsymbol{\tau})}{\partial \boldsymbol{\tau}} = \begin{bmatrix} -\left(\sigma_y\sigma_z - \tau_{yz}^2\right) + \frac{1}{3}\mathrm{d}\left(p^3\eta_f\right)/\mathrm{d}p \\ -\left(\sigma_z\sigma_x - \tau_{zx}^2\right) + \frac{1}{3}\mathrm{d}\left(p^3\eta_f\right)/\mathrm{d}p \\ -\left(\sigma_x\sigma_y - \tau_{xy}^2\right) + \frac{1}{3}\mathrm{d}\left(p^3\eta_f\right)/\mathrm{d}p \\ -2(\tau_{zx}\tau_{xy} - \sigma_x\tau_{yz}) \\ -2(\tau_{xy}\tau_{yz} - \sigma_y\tau_{zx}) \\ -2(\tau_{yz}\tau_{zx} - \sigma_z\tau_{xy}) \end{bmatrix} = \begin{bmatrix} -\left(\sigma_y\sigma_z - \tau_{yz}^2\right) + h_f p^2 \\ -\left(\sigma_z\sigma_x - \tau_{zx}^2\right) + h_f p^2 \\ -\left(\sigma_x\sigma_y - \tau_{xy}^2\right) + h_f p^2 \\ -2(\tau_{zx}\tau_{xy} - \sigma_x\tau_{yz}) \\ -2(\tau_{xy}\tau_{yz} - \sigma_y\tau_{zx}) \\ -2(\tau_{yz}\tau_{zx} - \sigma_z\tau_{xy}) \end{bmatrix} \tag{54}$$

where the non-dimensional factor h_f is defined as

$$h_f = \frac{1}{3p^2}\frac{\mathrm{d}}{\mathrm{d}p}\left(p^3\eta_f\right) = \left(1 + \frac{1}{3}m\right)\eta \tag{55}$$

Note, that in the differentiation $\eta_f(p)$ is the function defined by Eq. (16), while in the final form, η is determined directly from the condition $f(\boldsymbol{\sigma}) = 0$, whereby $\eta = I_3/p^3$.

A similar formula applies to the gradient of the flow potential (15), when the factor h_f is replaced by

$$h_g = \frac{1}{3p^2}\frac{\mathrm{d}}{\mathrm{d}p}\left(p^3\eta_g\right) = \left(1 + \left(1 + \frac{2}{3}n\right)\gamma\right)(1 - \gamma) \tag{56}$$

In the differentiation, $\eta_g = 1 - \gamma_g^2$, as given by Eq. (23), while in the final result $\gamma^2 = 1 - I_3/p^3$.

The elasto-plastic stiffness retains the format (39), when the elastic stiffness matrix (51) is used together with the yield and potential function gradients given by Eqs. (54)–(56).

5. Representative results

The model requires six parameters: two elastic stiffness parameters G and κ, the elasto-plastic stiffness λ, the plastic potential and yield function shape parameters n and m, and the non-dimensional weight parameter w in the plastic work. The latter three parameters can alternatively be specified in terms of the inclinations M_c, M_f and M_u illustrated in Fig. 7. Accurate representation of the behavior of granular materials as shown in Fig. 1, in particular the development of dilation, requires a non-linear calibration procedure as discussed by Ahadi and Krenk (1999).

The results of a non-linear calibration of the model parameters to standard triaxial test data for loose and dense sand are shown in Figs. 8 and 9. The two materials are loose Baskarp sand with an initial specific pore volume $e = 0.85$ (Borup and Hedegaard, 1995), and dense Lund sand with initial specific pore volume $e = 0.55$ (Ibsen and Jakobsen, 1996). In both tests, the initial isotropic confining pressure was $p_0 = 0.64$ MPa. The model parameters are given in Table 1. It is seen that for the dense sand, the

Table 1
Material parameters for Figs. 8–10

	G (MPa)	$\kappa \cdot 10^3$	$\lambda \cdot 10^3$	M_c	M_u	M_f
Loose sand	12.2	3.20	11.20	1.20	1.25	1.08
Dense sand	44.7	1.70	4.58	1.25	1.60	0.86

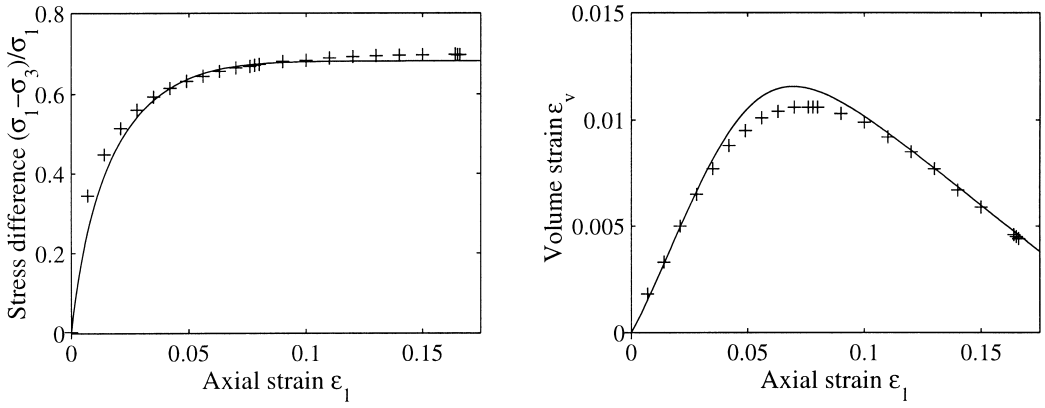

Fig. 8. Normalized stress and volumetric strain for Loose Baskarp sand.

shear stiffness G is nearly four times larger, and the elastic and elasto-plastic flexibilities κ and λ are two to three times smaller. Clearly, this gives smaller strains in the dense sand. However, a characteristic feature can also be observed for the parameters M_c, M_u and M_f. The inclination of the characteristic line M_c is quite similar for the two materials, and would probably be even closer for different packing of the same grains as illustrated in Fig. 1. For the loose sand, the ultimate state is only slightly above the characteristic state, implying that M_u is only slightly larger than M_c, while for the dense sand this difference is considerably larger. It turns out that a larger difference between M_u and M_c implies a larger difference between M_c and M_f.

The two sets of material parameters from Table 1 were used to predict the stress path in a triaxial constant volume (undrained) test with initial confining pressure $p_0 = 0.64$ MPa. Corresponding experimental results are not available for these materials, but the stress paths exhibit the correct qualitative behavior. The initial stress path, starting at the dashed isostatic line, is curved with the transverse stress component σ_3, decreasing until the characteristic state is reached. After a turn at the characteristic state, the stresses increase proportionally. The final part of the stress path lies between the

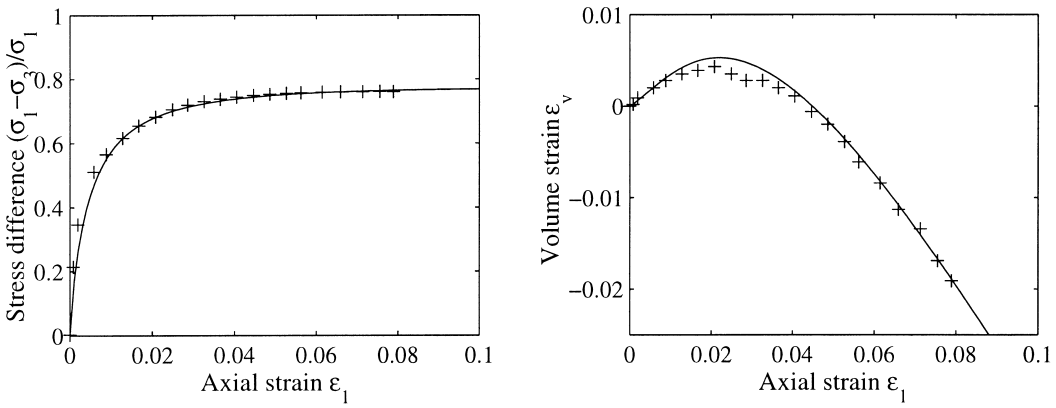

Fig. 9. Normalized stress and volumetric strain for Dense Lund sand.

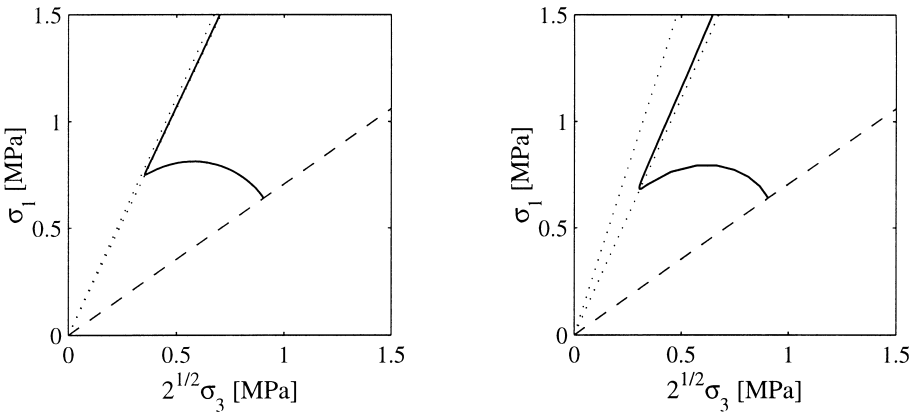

Fig. 10. Constant volume test predictions. (a) loose Barskap sand from Fig. 8, (b) dense Lund sand from Fig. 9.

characteristic and ultimate lines, described by

$$\sigma_1 = \frac{3+2M}{3-M}\sigma_3, \quad M = M_c, M_u \tag{57}$$

and shown as dotted lines in Fig. 10. The angle between the characteristic and ultimate lines is larger for dense materials, and generally this leads to a more smooth transition around the characteristic state for dense materials. However, the ratio between the stress components on the final part of the stress path depends on the ratio of elastic to plastic volume stiffness λ/κ as described by Ahadi and Krenk (1999).

6. Conclusions

A fully three-dimensional, non-associated isotropic hardening plasticity model for granular materials has been developed by combining yield function and flow potential families that fill the compression octant in principal stress space, a simple non-linear elasticity relation, and a weighted plastic work hardening rule. The common surface format for yield function and flow potential fills the principal stress octant such that, surfaces become increasingly triangular as they approach the principal stress coordinate planes. The shape of the flow potential is obtained from an approximate notion of the work of friction in the triaxial shear stress plane, leading to a pointed yield surface somewhat similar to that of the original Cam–Clay model (Schofield and Wroth, 1968), but consistently located fully inside the compression octant of principal stress space.

The model is described in terms of only six parameters: G and κ for elastic stiffness, λ for elasto-plastic stiffness, the two surface shape parameters n and m, and a non-dimensional weight w determining the ratio between the components of the plastic strain increments at failure. This is an important generalization of the Cam–Clay model, in which, the characteristic state is assumed to be identical with the ultimate state, and therefore non-dilating. The gradient of the flow potential relates the ratio of the stress components and the direction of the plastic strain increments at the ultimate state, and thus, the single parameter w determines both properties. Both stress and strain increment ratio at the ultimate state are well predicted for the experimental results in Figs. 8 and 9, and further results analyzed by Ahadi and Krenk (1999), thus supporting the dual role of the parameter w in the model.

The model parameters can be obtained from a standard triaxial test by a non-linear procedure

described by Ahadi and Krenk (1999), where numerous test results for sand in standard or constant volume triaxial tests have been analyzed. The simple elasticity model, in which the tangent bulk modulus is assumed to be proportional to mean stress p, is found to be adequate for calibration of individual tests. However, a generalization of the model is needed, in order to correctly model the dependence of model parameters on initial void ratio.

Acknowledgements

Financial support from the Danish Technical Research Council and the Swedish Technical Research Council is gratefully acknowledged.

References

Ahadi, A., Krenk, S., 1999. Characteristic state plasticity for granular materials. Part II: Model calibration and results. International Journal of Solids and Structures 37, 6361–6380.

Andersen, A.T., Madsen, E.B., Schaarup-Jensen, A.L., 1997. Constitutive Modelling in Soil Mechanics. Masters thesis, Building Technology and Structural Engineering, Aalborg University, Aalborg, Denmark.

Borup, M., Hedegaard, J., 1995. Data Report 9403, Baskarp Sand No. 15, Geotechnical Engineering Group, Aalborg University, Aalborg, Denmark.

de Jong, Josselin., 1976. Rowe's stress dilatancy relation based on friction. Geotechnique 26, 527–534.

Haythornwaithe, R.M., 1984. A smooth yield surface consistent with triaxial test data. Mechanics Research Communications 11, 281–284.

Haythornwaithe, R.M., 1985. A family of smooth yield surfaces. Mechanics Research Communications 12, 87–91.

Haythornwaithe, R.M., 1992. Isotropic yield criteria developed from simple shear. Mechanics Research Communications 19, 59–64.

Ibsen, L.B., Jakobsen, F.R., 1996. Data Report, Lund Sand No. 0, Part 1, Geotechnical Engineering Group, Aalborg University, Aalborg, Denmark.

Krenk, S., 1996. A family of invariant stress surfaces. Journal of Engineering Mechanics 122, 201–208.

Krenk, S., 1997. A characteristic state plasticity model for granular materials. In: Fleck, N.A., Cocks, A.C.F. (Eds.), IUTAM Symposium on Mechanics of Granular and Porous Materials. Kluwer Academic Publishers, Dordrecht, pp. 83–94.

Krenk, S., 1998. Friction, dilation and plastic flow potential. In: Herrmann, H.J., Hovi, J.-P., Ludig, S. (Eds.), Physics of Dry Granular Media. Kluwer Academic Publishers, Dordrecht, pp. 255–260.

Lade, P.V., Duncan, J.M., 1975. Elasto-plastic stress–strain theory for cohesionless soil. Journal of the Geotechnical Engineering Division, ASCE 101 (GT10), 1037–1053.

Lade, P.V., 1977. Elasto-plastic stress–strain theory for cohesionless soil with curved yield surfaces. International Journal of Solids and Structures 13, 1019–1035.

Lade, P.V., Kim, M.K., 1995. Single hardening constitutive model for soil, rock and concrete. International Journal of Solids and Structures 32, 1963–1978.

Matsuoka, H., Nakai, T., 1985. Relationship among Tresca, Mohr–Coulomb and Matsuoka–Nakai failure criteria. Soils and Foundations 25, 123–128.

Roscoe, K.H., Burland, J.B., 1968. On the generalized behaviour of "wet" clay. In: Heyman, J., Leckie, F.A. (Eds.), Engineering Plasticity. Cambridge University Press, Cambridge, pp. 535–609.

Roscoe, K.H., Schofield, A.N., 1963. Mechanical behaviour of an idealized "wet" clay. In: Proceedings of the European Conference on Soil Mechanics and Foundation Engineering, Wiesbaden, 47–54.

Rowe, P.V., 1962. The stress-dilatancy relation for static equilibrium of an assembly of particles in contact. Proceedings of the Royal Society, London A269, 500–527.

Schofield, A.N., Wroth, C.P., 1968. Critical State Soil Mechanics. McGraw-Hill, New York.

Weidner, J., 1990., Vergleich von Stoffgesetzen granularer Schüttgüter zur Silodruckermittlung. Dr. Ing. dissertation, University of Karlsruhe, Karlsruhe, Germany.